Hindawi
Advances in Civil Engineering
Volume 2019, Article ID 9649165, 11 pages
https://doi.org/10.1155/2019/9649165

Research Article

The Mechanical Properties of Granite under Ultrasonic Vibration

Yu Zhou, Qiongqiong Tang, Shulei Zhang, and Dajun Zhao

Complex Condition Drilling Experiment Center, Jilin University, 130012 Changchun, China

Correspondence should be addressed to Dajun Zhao; 1729333689@qq.com

Received 3 October 2018; Accepted 3 December 2018; Published 20 January 2019

Academic Editor: Hui Yao

The new technique of using ultrasonic vibration to break hard rock is still in the experimental stage, but it has significant potential for improving the efficiency of hard rock crushing. We have analyzed the mechanical properties of granite under ultrasonic vibration and the characteristics of the damage produced. This was achieved by using an ultraloading device to apply continuous and discontinuous ultrasonic vibrations, respectively, to 32 mm diameter and 72 mm high granite samples. An ultradynamic data acceptor combined with strain gauges was used to monitor the strain of the granite in real time, and the elastic-plastic deformation behavior of the granite under ultrasonic vibration was observed. The results of this experiment indicate that the granite samples underwent elastic deformation, plastic deformation, and damage during this process. The samples first experienced compressive deformation with no obvious rupturing. As the vibration continued, the deformation finally became tensile, and significant fragmentation occurred. The mechanical properties of granite under ultrasonic vibration are analyzed in detail on the basis of these results, and the basis for selecting a vibration frequency is discussed.

1. Introduction

Due to the high strength of hard rock and its widespread distribution in deep strata, there is a common need for a means of rapidly breaking hard rocks for engineering projects such as tunneling and drilling [1–3]. A technology called "resonance breaking" that utilizes ultrasonic vibration has been developed for this purpose. The NASA designed a high-axial force ultrasonic drilling sampler for planetary exploration and ice-drilling, consisting of piezoelectric transducers, free mass blocks, and a drill bit [4–9]. Wiercigroch et al. [10, 11] applied the ultrasonic vibration technique to improve the efficiency of hard rock drilling and conducted a variety of experiments to ascertain the effect of ultrasonic vibration on rock fragmentation. Their investigations showed that ultrahigh-frequency axial vibration can significantly enhance drilling rates compared to the traditional rotary-type method [12]. Pavlovskaia et al. [13] concluded that a low-dimensional model provides good estimates for the optimal static force and the amplitude of the dynamic force and that this model can be used for the operational control of the drilling system, with the loading parameters being adjusted to achieve a resonant situation while drilling through different formations. Zhao [14] developed a simple nonlinear 2-DOFs (degrees of freedom) mass-spring model that can be used to analyze the process of dynamic cutting with normal ultrasonic vibration excitation. A compressive strength experiment was used to demonstrate that this technique can rapidly reduce the strength of hard granite rock, and CT scanning was used to examine the effect of static pressure on rock-breaking efficiency [15]. The results indicated that a threshold of static pressure exists for this method, and samples will become damaged when the static pressure exceeds this threshold. However, the abovementioned investigations mainly focused on parameter selection for the ultrasonic vibration technology, and the mechanical properties of granite under ultrasonic vibration, which are of significance for understanding the rock mechanics of ultrasonic vibration breaking, have rarely been studied.

Many investigations have focused on the mechanical properties of rock under cyclic loading. A summary of relevant research on various rock types is provided in Table 1. Experimental results have clearly demonstrated that damage gradually accumulates in rocks undergoing cyclic loading [16, 17]. It has also been found that the mechanical properties of rock are significantly affected by the loading parameters. Of these, the most important are the loading

Table 1: Summary of work related to fatigue behavior on rock.

Rock type	Loading type	Reference
Graywacke	Dynamic uniaxial cyclic loading ($f = 1$ Hz)	[16]
White Tennessee marble, Indiana limestone, Berea sandstone, Westerly granite	Triangular, uniaxial tension/compression cyclic loading ($f = 1$ Hz)	[17]
Artificial rock	Triaxial cyclic compressive loading ($f = 1$ Hz)	
Carboniferous sandstone	Sinusoidal cyclic compressive loading ($f = 0.1$, 1, and 10 Hz)	[18]
Salt rock	Uniaxial cyclic loading ($f = 0.001$–0.03 Hz)	[19]
Sandstone	Sinusoidal cyclic compressive loading ($f = 1$ Hz)	[20]
Salt rock	Triaxial cyclic compressive loading	[21]
Salt rock	Triaxial cyclic compressive loading with confining pressure ($f = 1$ Hz)	[22]
Sandstone	Cyclic loading (increased loading)	[23]
Coal	Cyclic loading	[24]
Lingnan gold mine	Triaxial cyclic loading	[25]
Concrete	Cyclic loading	[26]
Green Onyx	Fully reversed loading (1.5, 4.2, 6.4, 8.4, and 13 Hz)	[27]
Granodiorite, sandstone	Constant and stepped cyclic loading ($f = 1$ Hz)	[28]

rate, frequency, and stress amplitude [18, 29]. Rocks are more easily damaged at low frequencies and high amplitude than at high frequencies and low amplitude for a given energy input [19]. The effect of loading frequency on the rock strength appears to be small compared to the stress magnitude at low frequencies [20, 22, 28, 30]. Additionally, theoretical work has been conducted on rock fatigue. Xie et al. [31] discussed the relationships between energy dissipation and strength and energy release and global failure during the deformation and failure of a rock mass. Li et al. [24] investigated the classification and fractal characteristics of coal rock fragments under uniaxial cyclic loading and found that as the loading rate increased, the specimens were crushed more thoroughly and the fragments became more uniform in length, width, thickness, and overall size. You et al. [25] concluded that the elastic energy index increases as damage increases.

Deformational behavior is another important theme in investigating the mechanical properties of rock under cyclic loading. For example, it has been found that strain data can reflect the process of crack development in cyclic tests and that crack closure accompanies compressive deformation [32]. Liu et al. and Chen et al. [21, 23] studied the types of deformation that occurred during the loading process and concluded that their rock samples showed near-elastic behavior during initial cyclic loading but began to exhibit elastic-plastic behavior with an increase in the number of cycles. Furthermore, they found that the residual stress became larger along with an increase in loading stress. Another study used a modified Burger model to describe the creep behavior of red sandstone subjected to cyclic loading [33], and on the basis of acoustic emission monitoring, another study showed that the progressive damage caused by cyclic loading can be divided into crack damage and plastic damage [26]. Song et al. [27], meanwhile, showed that the S-N curves of rock samples were consistent with those observed in other brittle materials such as ceramics.

The abovementioned studies all focused on the mechanical properties of rock under conventional low-frequency cyclic loading. It has been found that the effect of this process on the mechanical properties of rock is related to the loading frequency, and many investigators have concluded that the response of rock materials under external harmonic excitation will change with loading frequency [34–36]. Thus, when ultrasonic vibration with a frequency in the same order of magnitude as the natural frequency of hard rock [37, 38] is applied to rocks, the mechanical properties of the rock should differ from those under conventional low-frequency cyclic loading. Thus, a comprehensive study of the mechanical properties of rock subjected to ultrasonic vibration is of great significance.

In this study, we analyzed the mechanical properties of granite, the characteristics of its deformation, the influence of vibration frequency, and the development of damage under ultrasonic vibration with a continuous and discontinuous loading path, constructing S-T (strain-time) curves. Due to the high frequency of ultrasonic vibration, there is a need to monitor the strain data dynamically. An advanced apparatus consisting of an ultradynamic data acceptor and strain gauges was therefore used. Our results will be conducive to a better understanding of fragmentation mechanisms under ultrasonic vibration and will provide theoretical guidance for the ultrasonic vibration technology.

2. Experimental Methods

2.1. Sample Preparation. The rock samples used in the experiments were processed from fine granite, a common type of hard rock in strata. The mineralogical composition of the rock was determined by X-ray diffraction (XRD). A Rigaku D/Max 2500 Cu radiation powder diffractometer was used, with the scanning conditions set to 2θ angles of 10°–90°, a scan step size of 0.02°, a scanning rate of 0.12°/s in the continuous mode, and a beam intensity of 50 kV and 200 mA. The XRD result, shown in Figure 1, indicates that the main components of the rock are quartz, albite, orthoclase, and hydrobiotite, indicating that the rock material is highly anisotropic. The samples were cut into standard

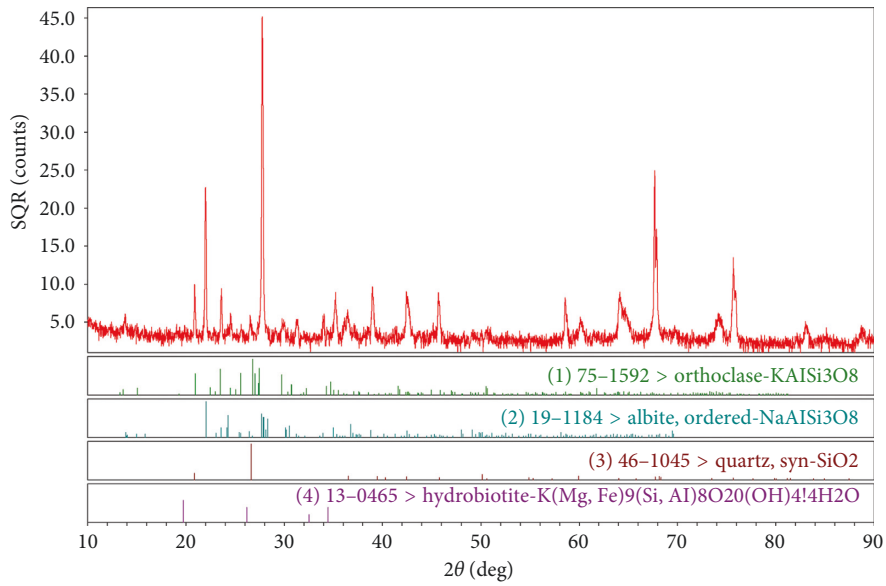

Figure 1: XRD result.

cylindrical blocks with a diameter of 36 mm and a height of 72 mm. In order to reduce the effect of heterogeneity on the experimental results, the samples were tested using the knocking method to examine their natural frequencies [39]. Samples with similar natural frequencies (26-27 kHz; Figure 2) were then selected for the subsequent experiments. Table 2 shows the mechanical parameters of the granite samples. These parameters were obtained through uniaxial compression tests, direct shear tests, and natural frequency tests.

2.2. Test Setup. The test equipment, as shown in Figure 3(a), comprises an ultrasonic vibration device and a strain data acquisition device. The vibration apparatus is composed of an ultrasonic power source (1), an ultrasonic vibrator (2), and a static loading device (3). The ultrasonic vibrator can excite vibration at frequencies of 30 kHz, 35 kHz, and 40 kHz. The strain data collection device was controlled using a computer (5), and an ultradynamic data acceptor (4) combined with four strain gauges placed on top of the sample (6) was used to collect strain data in real time. The loading method is shown in Figure 3(b). An ultrasonic dynamic load combined with a vertical static load was applied to the samples.

In the strain test, four strain gauges were placed on each sample to test the axial strain (A1 and A2) and the radial strain (R1 and R2). The height of A1 and R1 was Height 1 (H1) and the height of A2 and R2 was Height 2 (H2), where H1>H2. The specific locations of the strain gauges can be seen in Figure 3(a).

In order to analyze the mechanical properties of the rock samples, we designed a continuous vibration strain experiment and a discontinuous vibration strain experiment. The continuous test enabled the overall deformation law of the samples to be determined, while the discontinuous test allowed quantitative analysis of the elastic and plastic

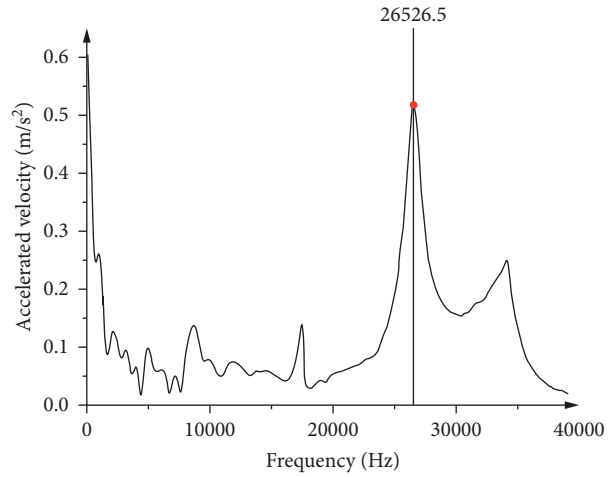

Figure 2: Natural frequency of the rock sample.

Table 2: Mechanical properties of the granite samples.

Modulus of elasticity (GPa)	Density (kg/m^3)	Compression strength (MPa)	Tensile strength (MPa)	Natural frequency (kHz)
52.3 ± 12.2	2790	116 ± 19	8.1 ± 1.5	26 ± 1

deformation. The two loading paths are shown in Figure 4, in which Δt is the time interval. $\Delta t = 0$ in the continuous test, and Δt represents the time from the discontinuation of vibration to the stabilization of the strain data in the discontinuous test.

The detailed experimental arrangements are as follows:

(1) For the continuous experiment, the granite samples were divided into three groups of five samples. The three groups were subjected to applied static loading of 200 N with ultrasonic vibration frequencies of 30 kHz, 35 kHz, and 40 kHz, respectively. We

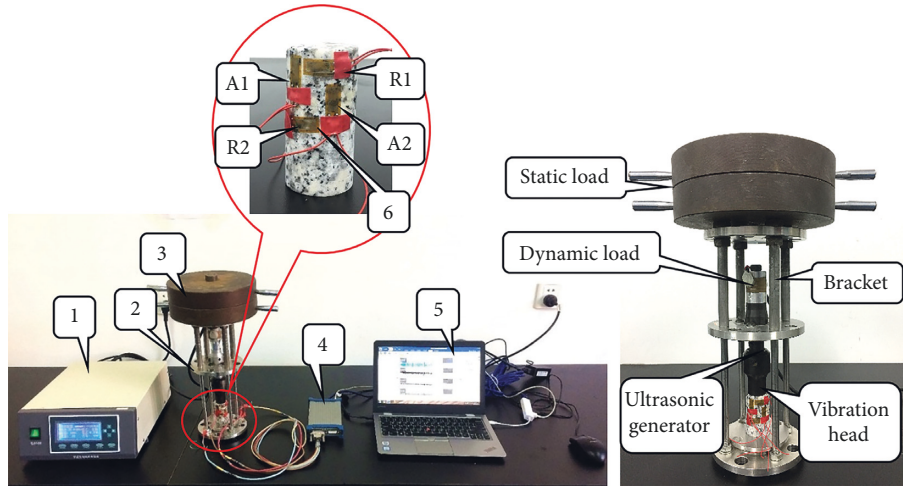

Figure 3: Ultrasonic vibration test. (a) Ultrasonic vibration and strain testing equipment. (b) Loading method.

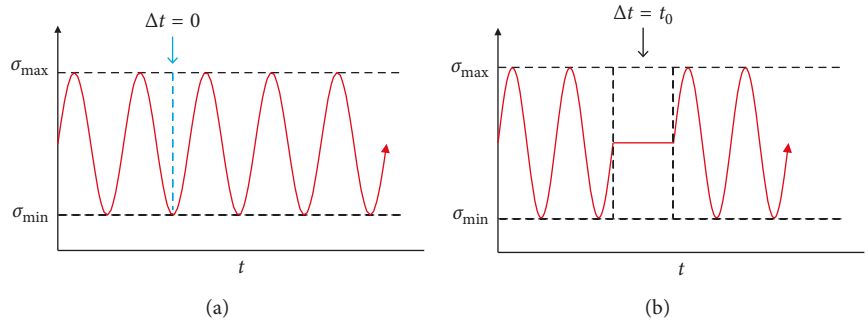

Figure 4: Loading path. (a) Continuous loading path. (b) Discontinuous loading path.

recorded the strain of the rock samples until the rock began to crack.

(2) For the discontinuous experiment, we tested the axial and radial strain at H1 of 10 samples under a static loading of 200 N. The frequency found to have the best crushing effect in the continuous tests was then selected as the discontinuous vibration parameter. During discontinuous vibration testing, the duration of each vibration ranged from 8 s to 30 s, after which the device was stopped until the monitoring system indicated that the strain curve had become stable. We repeated this process until fragmentation of the sample became evident. All experiments were conducted at room temperature.

3. Experimental Results and Analysis

3.1. Continuous Vibration Strain Test. The development of rock damage mainly manifested as macroscopic deformation. The magnitude of macroscopic deformation increases when cracks develop inside rock, and with a decrease in deformation, the cracks close [32]. Figure 5 shows a representative example of the results obtained for axial, radial, and volumetric strain versus vibration time. The figure shows that strain initially decreased at a steadily decreasing rate (the yellow, green, and blue lines in Figure 5(a) indicate the strain curve slope). The slopes of the strain curves were close to zero (with small fluctuations) at 120 seconds for the axial direction and 140 seconds for the radial direction, which means that the deformation barely changed in this period. And after this stable stage, the strain values increased as the vibration time increased. The strain versus vibration time curve is U-shaped, indicating that internal rock cracks mostly closed during the early period of vibration, and the compressive velocity of the sample gradually decreased. After a certain period of time, the strain tended to stabilize when the degree of crack closure became comparable to the degree of initiation and propagation of cracks. In the third stage, cracks mostly expanded as the rock dilated until destruction. However, the laws of strain in different directions and at different heights were not exactly the same. The results plotted in Figures 5(a)–5(c) show that the time taken for samples to compress to their limit along the axial direction was shorter than that in the radial direction. Furthermore, the stable phase was shorter along the axial direction than that in the radial direction. These results indicate that cracks propagated more readily perpendicular to the loading direction of the ultrasonic vibration. The results in Figure 5(d) show that the absolute strain at H1 along both the axial and radial directions was larger than that

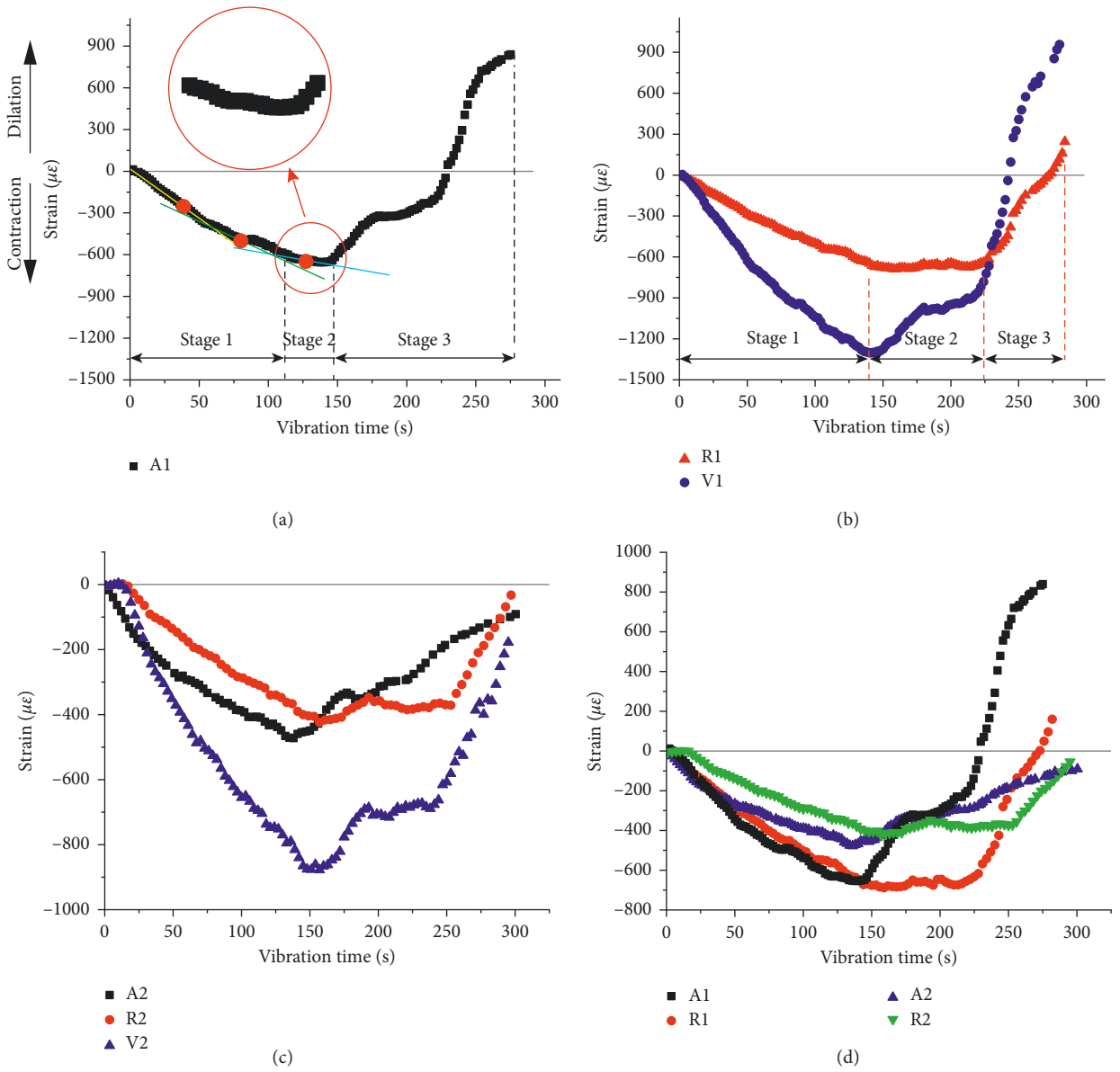

Figure 5: Strain data in the continuous vibration strain test. (a) Axial strain at H1. (b) Radial and volumetric strain at H1. (c) Axial, radial, and volumetric strain at H2. (d) Axial and radial strain at H1 and H2.

at H2. This difference was especially evident during the ascendant stage of strain when the rock cracked. The strain was positive at H1, while it was still negative at H2.

The entire failure process of the sample under ultrasonic vibration is shown in Figure 6. Firstly, there is a small amount of damage at the edge. Next, these small damaged zones connect with each other, and the damaged area becomes larger. Finally, the failure plane develops from the edge to the center quickly, and fragments produced in this process fly out of the sample (Figure 6(b)). The size distribution of the fragments produced in the tests is shown in Figure 6(c). There were several large fragments combined with smaller fragments and some fines, which is an indication of fatigue failure [30].

To investigate the effect of ultrasonic vibration frequency on breaking efficiency in more detail, we compared the axial strain at H1 of samples subjected to different vibration frequencies (Figure 7). The results show that the ultrasonic vibration frequency significantly influenced the deformation process. The strain rate is here indicated by the slope of the strain curve, and the absolute value of the strain rate in both the descendant and ascendant stages decreased in the order 30 kHz, 35 kHz, and 40 kHz. During the strain reduction stage, the strain rate at 30 kHz frequency was 255% and 599% greater than that at the 35 kHz and 40 kHz frequencies, respectively. When in the ascendant stage, that at 30 kHz frequency was 623% and 680% greater than that at 35 kHz and 40 kHz, respectively. Therefore, the time taken for the granite samples to break decreased in the order 40 kHz, 35 kHz, and 30 kHz. The vibration frequency selected for the discontinuous test was therefore 30 kHz.

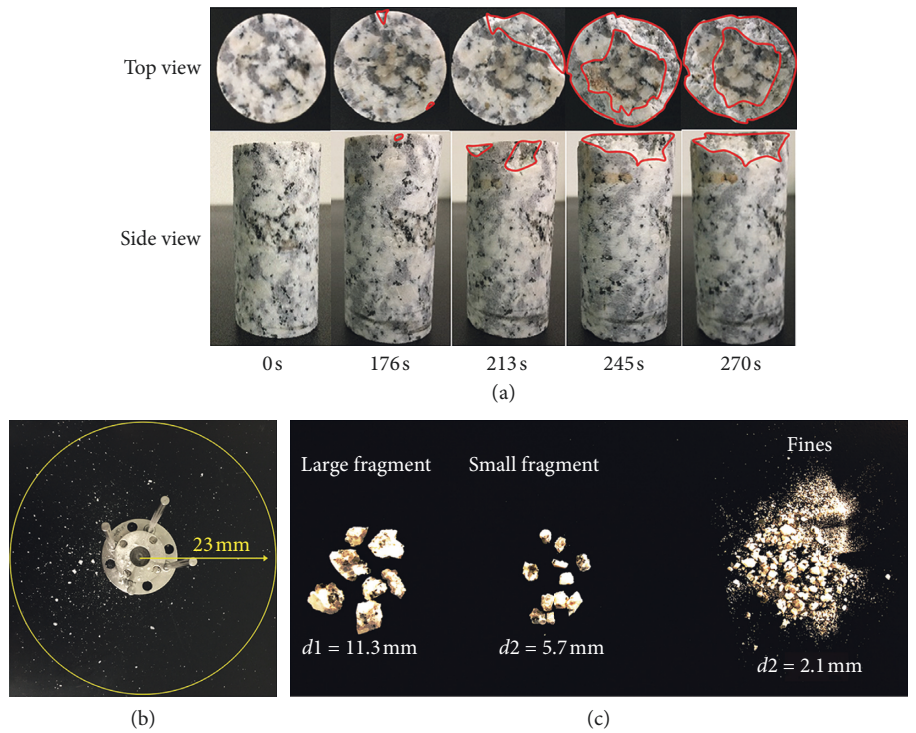

FIGURE 6: Fracture mode of the samples. (a) Destruction process of samples (the red line area represents the destruction area). (b) Injection radius. (c) Fragments size distribution (the numbers mean the average sizes of three types of fragments).

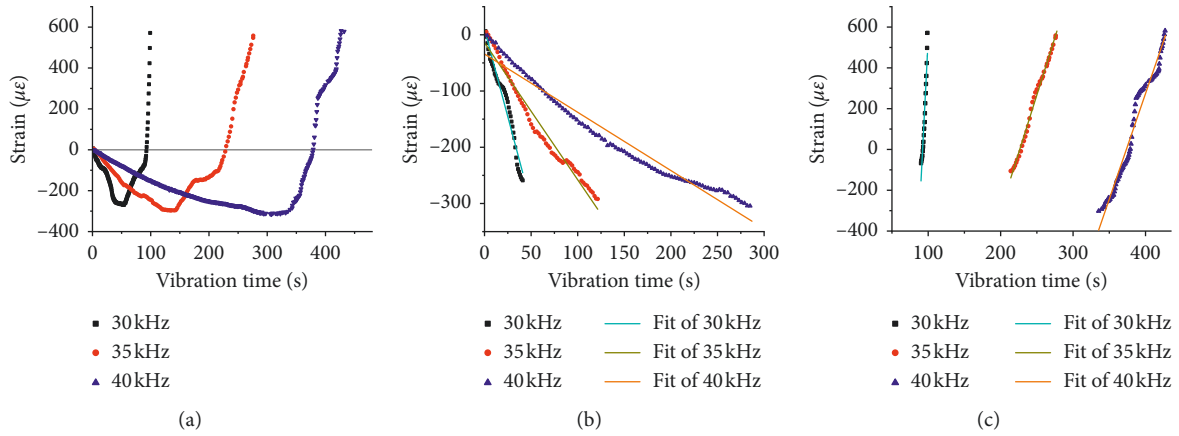

FIGURE 7: Strain of samples under ultrasonic vibration with different frequencies. (a) Whole strain process. (b) Descendant process of strain. (c) Ascendant process of strain.

3.2. Discontinuous Vibration Strain Test. The strain-time curve for the discontinuous vibration test is shown in Figure 8. In this experimental process, the sample began to crack after six intermittent vibrations. During the sixth vibration, the specimen expanded after it had been contracted for a period of time. Before the sixth vibration, the results indicated that the sample did not fully recover to its initial position after vibration. This illustrates that the deformation of samples under ultrasonic vibration can be decomposed into reversible and irreversible components. The distance between the stable strain line and the initial line on the curves represents the irreversible components, termed "residual strain." The results also indicated that, during the first five vibrations, the position of stable strain line was lower than the initial position after vibration had ceased. This result indicates that residual compressive strain was generated and that the sample suffered from residual compressive stress at the same time in both the radial and axial directions [40].

The reversible component was induced by the elasticity of the rock, while the irreversible component could be induced by plasticity and crack damage [41]. The development of residual strain in the granite sample is shown in Figure 9. Three stages of residual strain can be identified: (1) the uniform velocity phase, where residual compressive strain

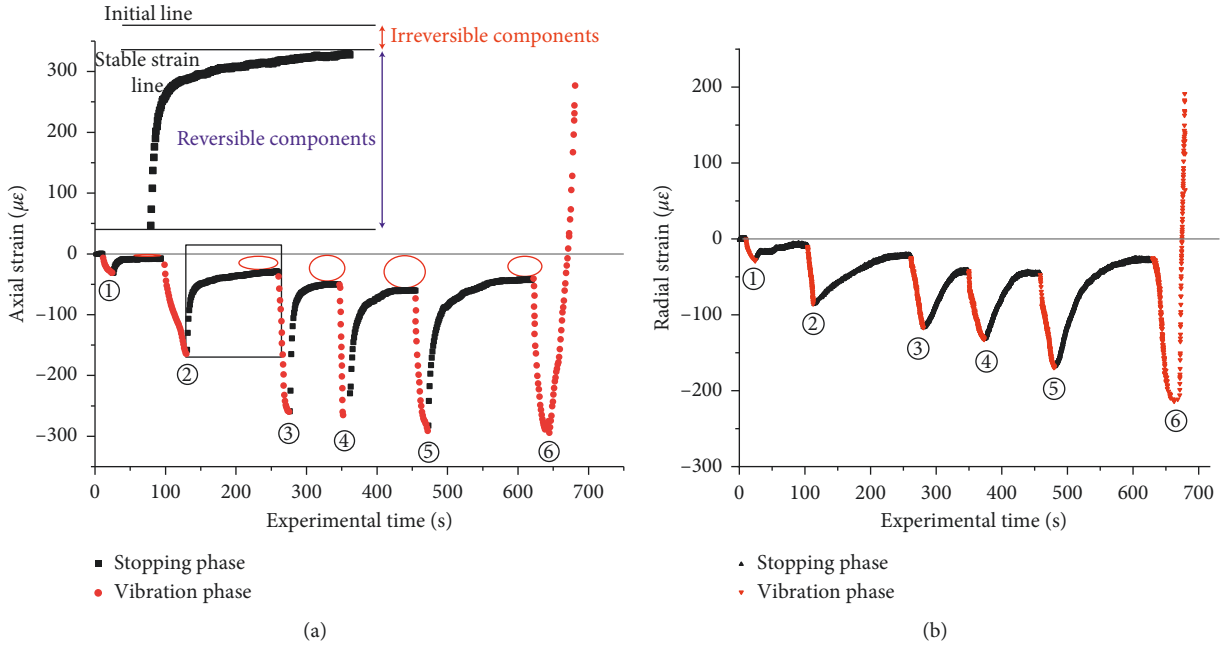

Figure 8: Strain of samples under the discontinuous ultrasonic vibration test. (a) Axial strain. (b) Radial strain.

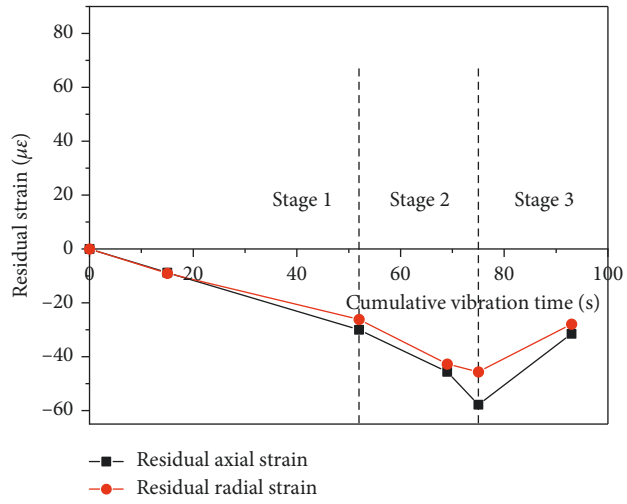

Figure 9: Development of residual strain and elastic strain during the vibration phase.

increases at a constant velocity; (2) the accelerated phase, where residual axial compressive deformation rapidly increases with increasing velocity; and (3) the reversed decrease phase, where residual axial compressive deformation decreases. In stages 1 and 2, the residual strain mostly resulted from plastic damage. In stage 3, crack damage had the largest effect on the residual strain value because crack generation can result in the expansion of the sample, which can, in turn, decrease the residual compressive strain.

4. Discussion

4.1. Mechanical Properties of Granite under Ultrasonic Vibration. Since granite is a highly anisotropic material, it contains a large number of internal joints and microcracks. On the one hand, when the energy wave meets a crack surface during the transmission of ultrasonic vibration energy, the energy wave will reflect [42], as shown in Figure 10. The reflected energy will result in radial vibration, and the nonreflected energy will continue to propagate along the axial direction. On the other hand, the ultrasonic vibration will introduce residual compressive stress due to the inhomogeneous deformation caused by the high anisotropy of granite, and this is confirmed by the discontinuous ultrasonic vibration experiment results. This finding, the first such observation for rock material subjected to ultrasonic vibration, is in good agreement with the results of ultrasonic vibration experiments performed by Ding et al. and Uhlmann on nonmetallic brittle material such as glass and ceramic materials [43, 44]. Therefore, during the cyclic process, the external applied stress will superimpose the internal residual stress inside the specimen in both the axial and radial directions. The stress distribution after superposition is shown in Figure 11. The generation of residual stress leads to a reduction in the stress ratio.

Since almost no new cracks are generated inside the rock in stage 1, the deformation of the rock at this time was mainly caused by the superimposed stress. Because of the reduced stress ratio, the degree of contraction during each cycle was larger than that of expansion, and the rock was squeezed in both the axial and radial directions. Therefore, both the radial and axial strains decreased and cracks closed as a whole during this stage [32]. As the vibration continued, new cracks were gradually generated, which led to an increase in expansion. The strain rate then gradually decreased, and it entered stage 2 when strain became essentially unchanging. As the cracks continued to expand, the magnitude of the expansion deformation caused by crack

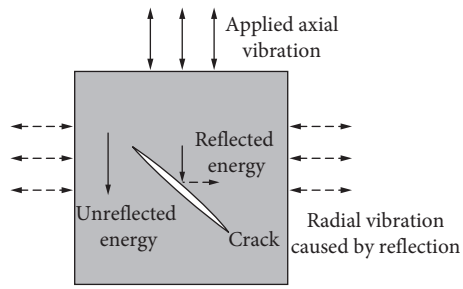

Figure 10: Ultrasonic energy propagation process.

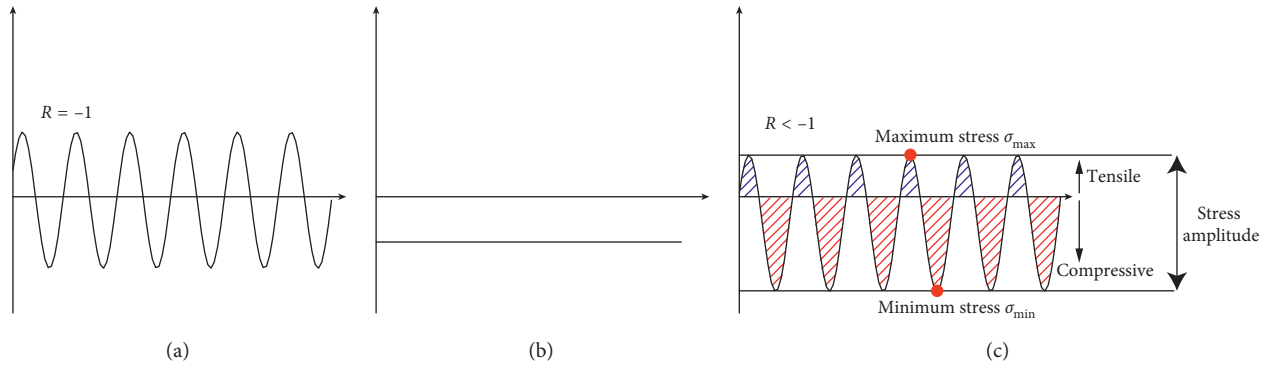

Figure 11: Stress distribution after superimposing applied stress and residual compressive stress (R is the stress ratio, $R = \sigma_{min}/\sigma_{max}$). (a) Applied stress. (b) Residual stress. (c) Superimposed stress.

propagation became much larger than that of the contraction caused by superimposed stress. Thus, both the radial and axial strains increased in stage 3, and finally, the cracks interpenetrated and macroscopic damage occurred.

In the strain decrease stage, crack closure can change the internal structure of the rock [32, 35], which in turn can affect the response of the rock to ultrasonic vibration. When rock is subjected to a continuous harmonic external excitation, a steady-state response is generated in the rock as follows [35]:

$$B_d = \frac{A}{\sqrt{\left(1-\lambda^2\right)^2 + (2\zeta\lambda)^2}}, \quad (1)$$

where λ expresses the ratio of the harmonic force frequency over the natural frequency of the rock with $\lambda = \omega/\omega_n$; B_d is the displacement amplitude of the rock (m); ζ is the damping ratio; ω is the external excitation frequency (Hz); ω_n is the natural frequency of the rock (Hz); and A is the external loading amplitude. Thus, the displacement amplitude of rock will increase when the vibration frequency approaches its natural frequency.

By using the following equation, we analyzed the relationship between the natural frequency of the rock and the total length of cracks [36]:

$$\omega_n = \sqrt{\frac{aS}{L_y L m}}, \quad (2)$$

where L is the length of the rock sample (m), S is the cross-sectional area of the rock sample (m^2), L_y is the length parameter of the cracks (m), m is the rock sample mass (kg), and a is the surface energy per unit area (J). When cracks in the sample close, the total length of the cracks decreases and the overall natural frequency of the sample increases. According to Eq. (1), the displacement amplitude of the rock will therefore increase as the natural frequency of the rock approaches the frequency of ultrasonic vibration, which can accelerate the damage process [20, 22, 30].

We evaluate this finding by tracking the dynamic development of displacement amplitude based on the axial strain data in the continuous vibration test. Strain amplitude, which we define as the difference between the maximum and the minimum strain in each second (Figure 12(a)), can be used to reflect the displacement amplitude of the tested samples. A greater strain amplitude indicates a greater displacement amplitude, and vice versa. The evolution of strain amplitude in Figure 12(b) shows that, in the early period of vibration, the strain amplitude increased with continued vibration, indicating that the increase of the natural frequency caused by crack closure resulted in an increase in the displacement amplitude. When the rock had deformed to its compressive limit, the natural frequency also approached its maximum, and so did the displacement amplitude. The fatigue process will accelerate due to increased displacement [30, 35]. As the cracks subsequently expanded, the natural frequency decreased, and a decrease in the displacement amplitude occurred.

4.2. Effects of Vibration Frequency. The results of our study show that the frequency of vibration had a significant influence on the mechanical properties of the granite samples.

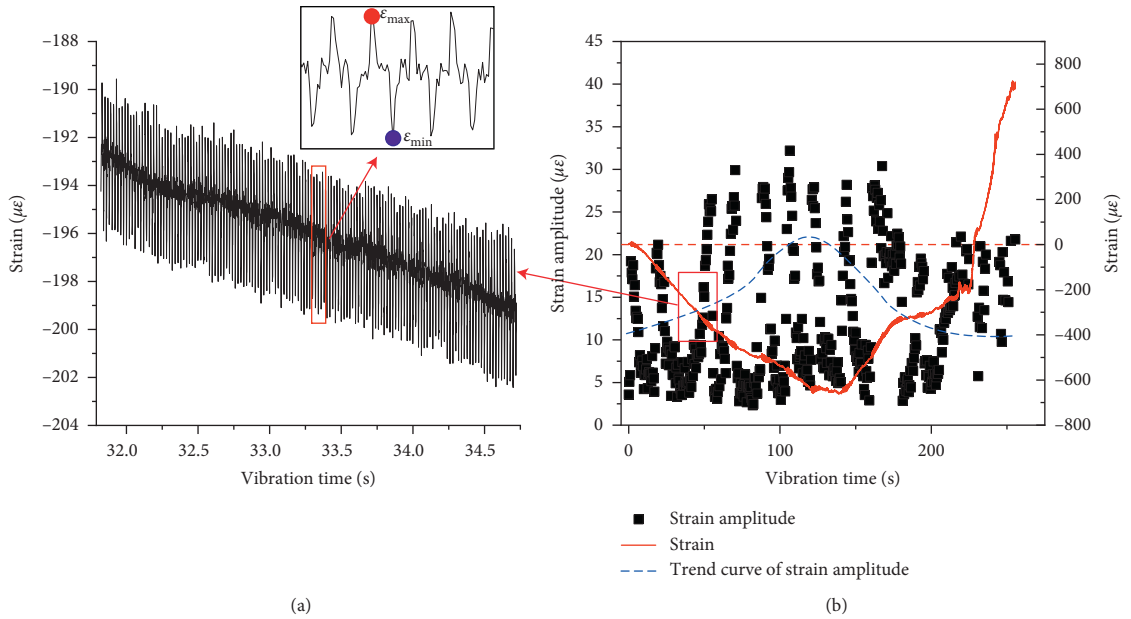

Figure 12: Change process of strain amplitude. (a) Detail of the strain data. (b) Development of strain amplitude and strain.

When the vibration frequency is close to the natural frequency of the sample, resonance will cause a significant increase in the displacement amplitude of the sample [35]. This can rapidly increase the crack propagation rate [45]. Therefore, when we applied ultrasonic vibration at 30 kHz to a granite sample with a natural frequency of nearly 30 kHz, destruction occurred significantly more rapidly than at 35 kHz or 40 kHz.

According to the analysis above, the natural frequency of the sample first increases and then decreases during the vibration process. In order to enable high crushing efficiency, the frequency of applied ultrasonic vibration needs to be within the range of the changing natural frequency of the rock.

5. Conclusions

In this study, we investigated the mechanical properties of granite under ultrasonic vibration. The following conclusions can be drawn from the experimental results:

(1) The samples underwent elastic deformation, plastic deformation, and damage during ultrasonic vibration. The samples deformed with the same trend in both the axial and radial directions. Contraction occurred initially, then deformation stabilized for a period, and this was followed by expansion until failure.

(2) In the volumetric compaction phase, the energy reflected when meeting cracks inside the sample caused the samples to suffer from both ultrasonic vibration in the radial and axial directions and the residual compressive stress generated by this process. Crack closure under the action of the superimposed stress caused the sample to contract. Crack closure causes the natural frequency of rock to increase, in turn increasing the displacement amplitude, which can accelerate the fatigue process. With crack initiation and propagation, the rate of contraction decreased, and the rock entered a stage of volumetric expansion in which the rock damage speed increased due to the significant effect of stress concentration.

(3) Vibration frequency had a significant influence on the mechanical properties of the granite samples. Since the natural frequency of rock first increases and then decreases during the process of applying vibration, it is necessary to enable high crushing efficiency to ensure that the frequency of the applied ultrasonic vibration is within the range of the changing natural frequency of the rock.

Further experimental work using methods such as the hole-drilling strain-gauge method and the ultrasonic nondestructive testing method, however, is required to validate the development of residual compressive stress under ultrasonic vibration quantitatively. Additionally, in order to observe the behavior of crack propagation, which is very hard to observe in physical experiments but is a very important factor for understanding the fragmentation mechanism with this technology, numerical simulation is necessary in the next study.

Data Availability

The data used to support the findings of this study are available from the corresponding author upon request.

Conflicts of Interest

The authors declare that they have no conflicts of interest.

Acknowledgments

This research was supported by the National Natural Science Foundation of China (4157020248), which is greatly appreciated.

References

[1] C. Zha, G. Liu, J. Li, Y. Li, Y. Xi, and B. Guo, "Combined percussive-rotary drilling to increase rate of penetration and life of drill bit in drilling hard rock formation," *Chemistry and Technology of Fuels and Oils*, vol. 53, no. 2, pp. 254–262, 2017.

[2] K. R. Hong and R. H. Yang, "The major problems and countermeasures on the shield machine tunneling in the hard rock stratum," *Applied Mechanics and Materials*, vol. 105–107, pp. 1438–1442, 2011.

[3] C. Zhu, Z. Tao, S. Yang, and Z. Shuai, "V shaped gully method for controlling rockfall on high-steep slopes in China," *Bulletin of Engineering Geology and the Environment*, pp. 1–17, 2018.

[4] Y. Bar-Cohen, X. Bao, Z. Chang, and S. Sherrit, "An ultrasonic sampler and sensor platform for in situ astrobiological exploration," in *Proceedings of Smart Structures and Materials 2003: Smart Structures and Integrated Systems*, pp. 457–465, San Diego, CA, USA, 2003.

[5] Y. Bar-Cohen, S. Sherrit, B. P. Dolgin et al., "Ultrasonic/sonic drilling/coring (USDC) for planetary applications," in *Proceedings of Smart Structures and Materials 2001: Smart Structures and Integrated Systems*, pp. 441–448, Newport Beach, CA, USA, 2001.

[6] BarCohen and Yoseph, *Ultrasonic/Sonic Mechanism of Deep Drilling (USMOD)*, 2005.

[7] S. Sherrit, X. Bao, Z. Chang et al., "Modeling of the ultrasonic/sonic driller/corer: USDC," in *Proceedings of Ultrasonics Symposium*, pp. 691–694, Puerto Rico, USA, 2000.

[8] S. Sherrit, B. P. Dolgin, Y. Bar-Cohen, D. Pal, J. Kroh, and T. Peterson, "Modeling of horns for sonic/ultrasonic applications," in *Proceedings of Ultrasonics Symposium*, pp. 647–651, Caesars Tahoe, NV, USA, 2000.

[9] B. Xiaoqi, B. C. Yoseph, C. Zensheu et al., "Modeling and computer simulation of ultrasonic/sonic driller/corer (USDC)," *IEEE Transactions on Ultrasonics Ferroelectrics & Frequency Control*, vol. 50, no. 9, p. 1147, 2003.

[10] M. Wiercigroch, *Resonance Enhanced Drilling: Method and Apparatus*, 2007.

[11] M. Wiercigroch, A. M. Krivtsov, and J. Wojewoda, "Dynamics of ultrasonic drilling of hard materials," in *Applied Nonlinear Dynamics and Chaos of Mechanical Systems with Discontinuities*, M. Wiercigroch and B. de Kraker, Eds., pp. 403–444, World Scientific, Singapore, 2000.

[12] M. Wiercigroch, J. Wojewoda, and A. M. Krivtsov, "Dynamics of ultrasonic percussive drilling of hard rocks," *Journal of Sound and Vibration*, vol. 280, no. 3–5, pp. 739–757, 2005.

[13] E. Pavlovskaia, D. C. Hendry, and M. Wiercigroch, "Modelling of high frequency vibro-impact drilling," *International Journal of Mechanical Sciences*, vol. 91, pp. 110–119, 2013.

[14] D. Zhao, "Dynamical analysis of drill bit with ultrasonic vibration," in *Proceedings of OMAE*, pp. 1–5, St. John's, Newfoundland, Canada, 2015.

[15] S. Yin, D. Zhao, and G. Zhai, "Investigation into the characteristics of rock damage caused by ultrasonic vibration," *International Journal of Rock Mechanics and Mining Sciences*, vol. 84, pp. 159–164, 2016.

[16] S. K. Singh, "Fatigue and strain hardening behaviour of graywacke from the flagstaff formation, New South Wales," *Engineering Geology*, vol. 26, no. 2, pp. 171–179, 1989.

[17] B. C. Haimson, "Effect of cyclic loading on rock," in *Dynamic Geotechnical Testing ASTM STP 654*, pp. 228–245, American Society for Testing and Materials, Philadelphia, PA, USA, 1978.

[18] M. K. Jafari, F. Pellet, M. Boulon, and K. A. Hosseini, "Experimental study of mechanical behaviour of rock joints under cyclic loading," *Rock Mechanics and Rock Engineering*, vol. 37, no. 1, pp. 3–23, 2004.

[19] M. N. Bagde and V. Petroš, "Fatigue properties of intact sandstone samples subjected to dynamic uniaxial cyclical loading," *International Journal of Rock Mechanics and Mining Sciences*, vol. 42, no. 2, pp. 237–250, 2005.

[20] K. Fuenkajorn and D. Phueakphum, "Effects of cyclic loading on mechanical properties of Maha Sarakham salt," *Engineering Geology*, vol. 112, no. 1–4, pp. 43–52, 2010.

[21] E. Liu and S. He, "Effects of cyclic dynamic loading on the mechanical properties of intact rock samples under confining pressure conditions," *Engineering Geology*, vol. 125, pp. 81–91, 2012.

[22] S. Ren, Y. Bai, J. Zhang, D. Jiang, and C. Yang, "Experimental investigation of the fatigue properties of salt rock," *International Journal of Rock Mechanics and Mining Sciences*, vol. 64, pp. 68–72, 2013.

[23] J. Chen, C. Du, D. Jiang, J. Fan, and Y. He, "The mechanical properties of rock salt under cyclic loading-unloading experiments," *Geomechanics and Engineering*, vol. 10, no. 3, pp. 325–334, 2016.

[24] Y. Li, S. Zhang, and X. Zhang, "Classification and fractal characteristics of coal rock fragments under uniaxial cyclic loading conditions," *Arabian Journal of Geosciences*, vol. 11, no. 9, 2018.

[25] S. You, H. Ji, Z. Zhang, and C. Zhang, "Damage evaluation for rock burst proneness of deep hard rock under triaxial cyclic loading," *Advances in Civil Engineering*, vol. 2018, Article ID 8193638, 7 pages, 2018.

[26] X. Wang, S. Wu, H. Ge, Y. Sun, and Q. Zhang, "The complexity of the fracture network in failure rock under cyclic loading and its characteristics in acoustic emission monitoring," *Journal of Geophysics and Engineering*, vol. 15, no. 5, pp. 2091–2103, 2018.

[27] Z. Song, T. Frühwirt, and H. Konietzky, "Characteristics of dissipated energy of concrete subjected to cyclic loading," *Construction and Building Materials*, vol. 168, pp. 47–60, 2018.

[28] H. Haghgouei, H. Hashemolhosseini, A. Baghbanan, and S. Jamali, "The effect of loading frequency on fatigue life of green onyx under fully reversed loading," *Experimental Techniques*, vol. 42, no. 1, pp. 105–113, 2017.

[29] X. Wang, Z. Wen, Y. Jiang, and H. Huang, "Experimental study on mechanical and acoustic emission characteristics of rock-like material under non-uniformly distributed loads," *Rock Mechanics and Rock Engineering*, vol. 51, no. 3, pp. 729–745, 2017.

[30] R. Geranmayeh Vaneghi, B. Ferdosi, A. D. Okoth, and B. Kuek, "Strength degradation of sandstone and granodiorite under uniaxial cyclic loading," *Journal of Rock Mechanics and Geotechnical Engineering*, vol. 10, no. 1, pp. 117–126, 2018.

[31] H. XIe, Y. Ju, L. Li, and R. Peng, "Energy mechanism of deformation and failure of rock masses," *Chinese Journal of Rock Mechanics and Engineering*, vol. 27, no. 9, pp. 1729–1740, 2008.

[32] X. Ge and Y. Lu, "Discussion on fatigue failure and irreversible deformation of rock under cyclic loading," *Journal of Geotechnical Engineering*, vol. 14, no. 3, pp. 56–60, 1992.

[33] B. Zhao, D. Liu, and W. Liu, "Mechanical behavior of sandstone under uniaxial constant cyclical compressive and

tensile loading," *Arabian Journal of Geosciences*, vol. 11, no. 17, 2018.

[34] S. Q. Li, T. Yan, W. Li, and F. Q. Bi, "Modeling of vibration response of rock by harmonic impact," *Journal of Natural Gas Science and Engineering*, vol. 23, pp. 90–96, 2015.

[35] W. Li, T. Yan, S. Li, and X. Zhang, "Rock fragmentation mechanisms and an experimental study of drilling tools during high-frequency harmonic vibration," *Petroleum Science*, vol. 10, no. 2, pp. 205–211, 2013.

[36] S. Li, T. Yan, W. Li, and F. Bi, "Simulation on vibration characteristics of fractured rock," *Rock Mechanics And Rock Engineering*, vol. 49, no. 2, pp. 515–521, 2015.

[37] S. W. Wang, Y. Lei, F. Lin, Z. Zheng, and W. Zheng, "Experimental study of rock frequency," *China Science and Technology Information*, vol. 22, no. 9, pp. 68-69, 2010.

[38] C. Hedberg, "Resonance frequency measurements of a few materials for temperature variations," in *Proceedings of Baltic-Nordic Acoustical Meeting*, Tallinn, Estonia, 2014.

[39] Y. Hu, M. Lv, S. Wang, and S. N. Abduljauwad, "Measurement of material natural frequency and elastic modulus by knocking method," *Mechanical Engineering & Automation*, vol. 39, no. 5, pp. 88-89, 2010.

[40] I. Nikitin and M. Besel, "Correlation between residual stress and plastic strain amplitude during low cycle fatigue of mechanically surface treated austenitic stainless steel AISI 304 and ferritic-pearlitic steel SAE 1045," *Materials Science and Engineering: A*, vol. 491, no. 1-2, pp. 297–303, 2008.

[41] D. Jiang, J. Fan, J. Chen, L. Li, and Y. Cui, "A mechanism of fatigue in salt under discontinuous cycle loading," *International Journal of Rock Mechanics and Mining Sciences*, vol. 86, pp. 255–260, 2016.

[42] L. Rose J and P. Nagy, *Ultrasonic Waves in Solid Media*, Cambridge University Press, Cambridge, UK, 2000.

[43] Y. Ding, A. Osaka, and Y. Miura, "Enhanced surface crystallization of β-barium borate on glass due to ultrasonic treatment," *Journal of The American Ceramic Society*, vol. 77, no. 3, pp. 749–752, 2010.

[44] E. Uhlmann and G. Spur, "Surface formation in creep feed grinding of advanced ceramics with and without ultrasonic assistance," *CIRP Annals*, vol. 47, no. 1, pp. 249–252, 1998.

[45] T. Chang, G. Li, and J. Hou, "Effects of applied stress level on plastic zone size and opening stress ratio of a fatigue crack," *International Journal of Fatigue*, vol. 27, no. 5, pp. 519–526, 2005.